Eur. Phys. J. D **20**, 499–511 (2002)
DOI: 10.1140/epjd/e2002-00148-5

THE EUROPEAN PHYSICAL JOURNAL D

N-acetyl-L-aspartic acid-N′-methylamide with side-chain orientation capable of external hydrogen bonding

Backbone and side-chain folding, studied at the DFT level of quantum theory

J.C.P. Koo[1,a], G.A. Chass[1,2,b], A. Perczel[3,c], Ö. Farkas[3,d], A. Varro[4], L.L. Torday[4,e], J.Gy. Papp[4,5,f], and I.G. Csizmadia[1,g]

[1] Department of Chemistry, University of Toronto, Toronto, Ontario, Canada M5S 3H6
[2] Velocet R & D, 210 Dundas St. West, Suite 810, Toronto, Ontario, Canada M5G 2E8
[3] Department of Organic Chemistry, Eotvos University, 1117 Budapest, Hungary
[4] Department of Pharmacology and Pharmacotherapy, Szeged University, Dom ter 12, 6701 Szeged, Hungary
[5] Division of Cardiovascular Pharmacology, Hungarian Academy of Sciences and Szeged University, Dom ter 12, 6701 Szeged, Hungary

Received 10 February 2002
Published online 13 September 2002 –

Abstract. In this study, we generated and analyzed the side-chain conformational potential energy hypersurfaces for each of the nine possible backbone conformers for N-acetyl-*L*-aspartic acid-N′ methylamide. We found a total of 27 out of the 81 possible conformers optimized at the B3LYP/6-31G(d) level of theory. The relative energies, as well as the stabilization energies exerted by the side-chain on the backbone, have been calculated for each of the 27 optimized conformers at this level of theory. Various backbone-backbone (N–H···O=C) and backbone-side-chain (N–H···O=C; N–H···OH) hydrogen bonds were analyzed. The appearance of the notoriously absent ε_L backbone conformer may be attributed to such side-chain-backbone (SC/BB) and backbone-backbone (BB/BB) hydrogen bonds.

PACS. 82.20.Wt Computational modeling; simulation

1 Introduction

1.1 Biological background

There exist a wide variety of proteins in all living entities. Some are regulatory proteins while others may be structural proteins. More interestingly, there is a group of proteins that bind to specific cell-surface receptors. Many of these adhesive proteins, such as fibrinogen, fibronectin, and collagens, contain the tripeptide sequence arginine-glycine-aspartic acid (RGD) which is the structural motif used for recognition by cell-surface receptors [1]. The RGD tripeptide has been intensely studied in molecular genetics, cell biology, as well as pharmacology. In recent years, gene therapy is an area of high interest in the medical fields. However, the effectiveness and expression of the target genes are often limited by the efficiency of the gene delivery system. The adenovirus vector has shown tremendous promise in efficient gene delivery for target genes [2,3]. Impressively, experiments showed that the RGD is important in expanding adenovirus vector tropism [4] as well as improving gene delivery efficiency [5,6]. In cancer research, studies have shown that RGD could trigger apoptosis [7] while showing low toxicity in antitumor activity against human lung cancer [8]. From these results, the RGD tripeptide shows that it has a great potential in clinical therapeutic studies. Interestingly, it was found that new RGD analogues, important for their transport properties in drug production, could enhance oral bioavailability [9]. However, it was emphasized

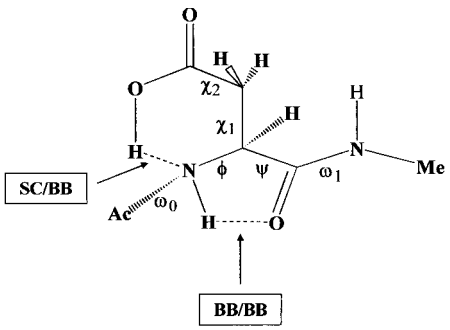

[a] e-mail: joseph.koo@utoronto.ca
[b] e-mail: gchass@fixy.org
[c] e-mail: perczel@para.chem.elite.hu
[d] e-mail: farkas@organ.elite.hu
[e] e-mail: pyro@phcol.szote.u-szeged.hu
[f] e-mail: papp@phcol.szote.u-szeged.hu
[g] e-mail: icsizmad@alchemy.chem.utoronto.ca

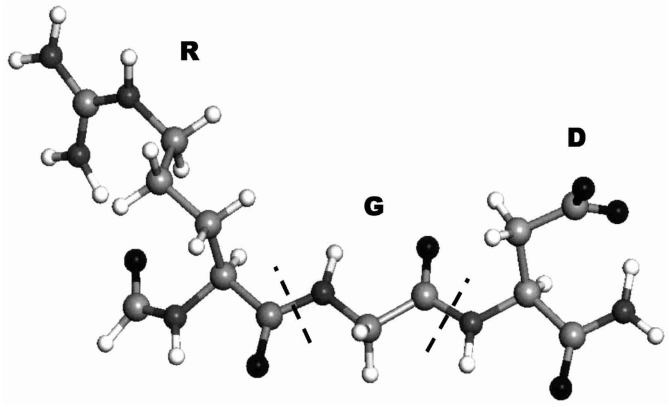

Fig. 1. An Arg-Gly-Asp (RGD) conformer obtained by preliminary optimization [48].

that the three dimensional conformation of the RGD must be thoroughly studied as it affects the peptides' hydrogen bonding ability as well as its molecular geometry [9].

One can examine the tripeptide RGD as three separate components, namely arginine (R), glycine (G), and aspartic acid (D) as shown in Figure 1. Glycine (G) has been studied very extensively through molecular computation. The focus of this paper is to explore the conformational variability of the aspartic acid (D) residue, whose conformation may affect, rather profoundly, the hydrogen bond formation as well as the molecular geometry of the RGD tripeptide.

The aspartic acid residue itself has shown tremendous biological applications. For instance, it was shown that if the *chemokine coreceptor CXCR4* of the human immunodeficiency virus-1 (HIV-1) has mutations in two of its aspartate regions, then its function of enhancing HIV-1 entry intro cells was greatly reduced [10]. Also, it was found that there exists aspartic acid-specific sites in *granzyme B* that are important in *cytotoxic T lymphocytes* and in the apoptosis-related caspase family [11]. In turn, these aspartic acid-specific sites allow for the probing of target proteins in their normal or disease states [11]. In neurology, the quantification of N-acetylaspartate, an aspartic acid residue, was shown to be a potential relative measurement of cellular dysfunction and neuronal loss for cerebral injury in stroke patients [12]. It has been shown that aspartic acid also plays a crucial role in protein decomposition [13], where its conformation directly influences the rate of racemization. In another experiment, carbonyl-carbonyl interactions, comparable to the energy of hydrogen bonds, were shown to provide stabilizing effects for aspartic acid and asparagines [14]. This experiment provides an explanation for which aspartic acid adopts conformations in certain regions of the Ramachandran plot ($\gamma_{\rm L}$, $\beta_{\rm L}$, $\delta_{\rm L}$, $\alpha_{\rm L}$, $\varepsilon_{\rm L}$, $\gamma_{\rm D}$, $\alpha_{\rm D}$) more readily than any other non-glycyl amino acids [14]. Other examples of aspartic acid-related studies include antibody selectivity [15], lipase activities [16], protein modification of aspartic acid bond isomerization in Alzheimer's Disease [17], enzyme kinetics in bacteria [18], antiproliferative activities for immunological studies [19], probing of HIV-1 protease binding site [20], gene sequences in mycobacterium's proteins [21], and functional roles in bacteriorhopdopsin [22]. In these studies, it is always reported that certain conformations of the aspartic acid are critical in the functionality of a system. In this paper, we wish to report all possible backbone (BB) and side-chain (SC) conformers that may exist for the aspartic acid residue in N-acetyl-*L*-aspartic acid N′-methylamide with a side-chain carboxyl group which is capable to intra- and inter-residual as well as intermolecular hydrogen bonding.

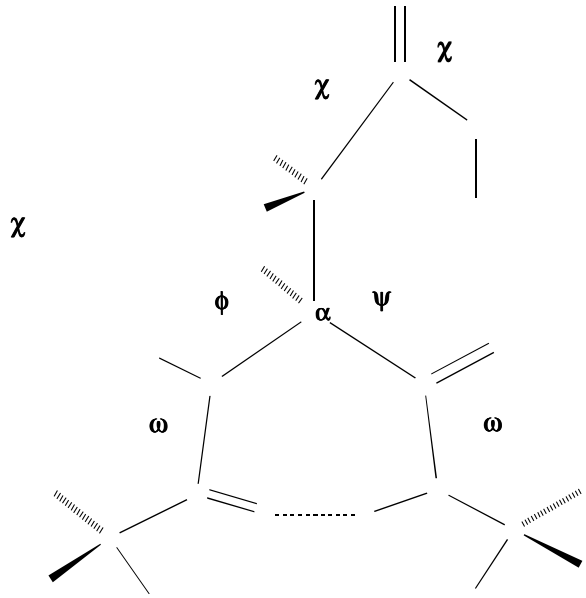

Fig. 2. Atomic numbering and definition of torsional angles for N-acetyl-*L*-aspartic acid N′-methylamide.

1.2 Stereo chemical background

N-acetyl-*L*-aspartic acid N′-methylamide, shown in Figure 2, has a methyl group in each of the N- and C-protective groups. This differs from N-formyl-*L*-aspartic acidamide, which has H atoms instead of methyl groups [23]. The backbone geometry of the aspartic acid residue is expected to be analogues to that of an alanine residue with the exception that a –COOH group has replaced one of the H atoms of the α-methyl group of alanine. In earlier studies on the alanine molecule [24–29], it was found that both the $\alpha_{\rm L}$ and $\varepsilon_{\rm L}$ backbone conformations, shown in Figure 3, did not exist. Since alanine is the simplest chiral amino acid having a backbone that other peptide residues also contain; it would not be surprising at all if the aspartic acid residue would not have stable geometries associated with the $\alpha_{\rm L}$ and $\varepsilon_{\rm L}$ backbone conformations. Besides alanine [24–29], various single amino acids have been subjected to *ab initio* calculation. These attempts include glycine [30,31], valine [32], phenylalanine [33–35], serine [36–38], asparagines [39], proline [40],

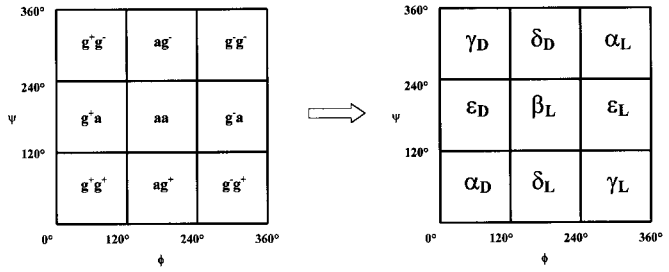

Fig. 3. Topology of a Ramachandran potential energy surface (PEHS), $E = E(\phi, \psi)$ of an amino acid residue in a peptide; (left) conformers are designated by IUPAC conventions; (right) conformers are designated by traditional conventions.

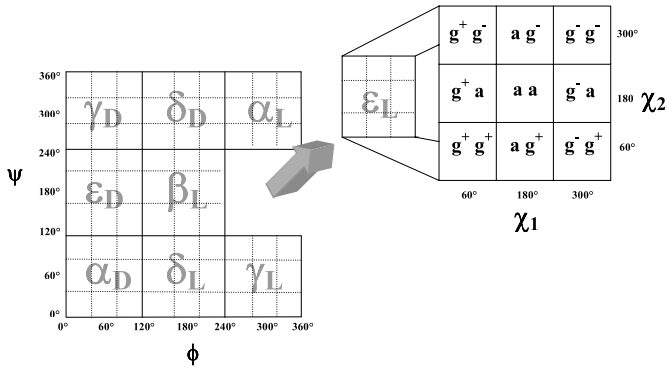

Fig. 4. A schematic representation of the 4D Ramachandran PEHS $E = E(\phi, \psi, \chi_1, \chi_2)$. Each of the nine backbone conformations (γ_L, β_L, δ_L, α_L, ε_L, γ_D, δ_D, α_D, and ε_D) has nine side-chain conformation as shown by the ε_L conformation.

cysteine [41] and selenocysteine [42]. Using alanine, extensive studies have been made on oligopeptides [43]. The present study includes the backbone (ϕ, ψ) and side-chain (χ_1, χ_2) variations leading to a 4D-Ramachandran potential energy hypersurface (PEHS): $E = E(\phi, \psi, \chi_1, \chi_2)$. Hence, on a 4D-Ramachandran PEHS, shown in Figure 4, $3^4 = 81$ geometries need to be optimized. The backbone conformations could lead up to $3^2 = 9$ structures (γ_L, β_L, δ_L, α_L, ε_L, γ_D, δ_D, α_D, and ε_D) on the 2D-Ramachandran map which are to be coupled with $3^2 = 9$ side-chain orientations.

Also, the N-acetyl-*L*-aspartic acid N′-methylamide side-chain, similar to N-formyl-*L*-aspartic acidamide [23], can be modeled by propionic acid [CH_3–CH_2–COOH] where CH_3 represents the α-carbon on the peptide residue. The internal H-bond within the carboxyl moiety appeared to be more stable both for the model propionic acid as well as for the aspartic acid residue. There exist two possible forms for the carboxyl group of the propionic acid side-chain: the *endo* form where $\chi_3 = 180°$ and the *exo* form where $\chi_3 = 0°$, shown in Figure 5. Due to this feature of the propionic acid side-chain, it is obvious that the aspartic acid residue, N-acetyl-*L*-aspartic acid N′-methylamide, also exists in both *endo* and *exo* forms. In this paper, we investigate the *exo* form of N-acetyl-*L*-aspartic acid N′-methylamide as it seems reasonable to assume that the *exo* form of propionic acid side-chain allows the aspartic

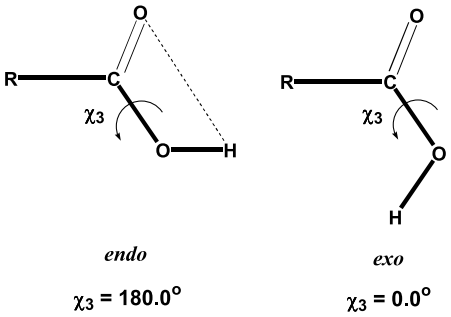

Fig. 5. Definitions of *endo* and *exo* conformations for the propionic side-chain of N-acetyl-*L*-aspartic acid N′-methylamide.

acid residue to form external hydrogen bonding. This external hydrogen bond formation may be biologically important, as it allows the aspartic acid residue to interact with other substrates, such as amino acid residues in proteins as well as with other substrates or ligands. If the propionic acid side-chain remains in the *endo* form, then the internal side-chain-side-chain hydrogen bonding can prevent the carboxyl group from forming external hydrogen bonds.

Prior to this research, Salpietro *et al.* [23] had performed a study to find the side-chain conformational potential energy surface, $E = E(\chi_1, \chi_2)$ of N-formyl-*L*-aspartic acidamide and its conjugate base N-formyl-*L*-aspartatamide in their γ_L backbone conformations. In that study, the parent amino acid diamide and its conjugate base with deprotonated side-chain were used to examine all side-chain conformations. Also, the side-chain in the neutral form and in the anionic conjugate base form, were mimicked using propionic acid and propionate ion.

We now explore the full backbone and side-chain conformational space with the *exo* orientation in the side-chain carboxylic acid moiety.

2 Computational methods

In this analysis, *ab initio* calculations were carried out using GAUSSIAN 94 [44] and GAUSSIAN 98 [45] on the nine backbone conformations (γ_L, β_L, δ_L, α_L, ε_L, γ_D, δ_D, α_D, and ε_D) for all possible conformers of N-acetyl-*L*-aspartic acid N′-methylamide. These *ab initio* calculations on the aspartic acid residue were used to determine its minima on the potential energy hyper surface (PEHS), as shown in Figure 4. The side-chain geometric characteristics can be related to propionic acid, CH_3–CH_2–COOH, where the carboxyl group, in its *exo* form shown in Figure 5, has a χ_3 of 0°. With these parameters, and under normal conditions where FOPT = Z-Matrix, partially relaxed PES scan calculations of the type: $E = E(\chi_1, \chi_2)$ were first performed on the *exo* form ($\chi_3 = 0°$) of N-acetyl-*L*-aspartic acid N′-methylamide. Consequently, all critical points for these scan calculations had gradients of less than 4.5×10^{-4} a.u. By specifying and restricting the ϕ and ψ (and of course, $\chi_3 = 0°$) torsional angles, the backbone of the *exo* aspartic acid residue were fixed to their respective backbone conformations (γ_L, β_L, δ_L, α_L, ε_L, γ_D, δ_D, α_D, and ε_D). Meanwhile, the two side-chain variables for

$$\underset{\substack{\gamma_L\\ -456.5375150\\ \text{hartree}}}{CH_3\text{–}CO\text{–}(NH\text{–}CH_2\text{–}CO)\text{–}NHCH_3} + \underset{\substack{\\ -268.3872059\\ \text{hartree}}}{CH_3\text{–}R} \rightarrow \underset{\text{any conformation}}{CH_3CO\text{–}(NH\text{–}CHR\text{–}CO)\text{–}NHCH_3} + \underset{\substack{\\ -40.5183829\\ \text{hartree}}}{CH_4 + \Delta E^{\text{stabil}}\,(\gamma_L)} \quad (1)$$

$$\underset{\substack{\beta_L\\ -456.5357122\\ \text{hartree}}}{CH_3\text{–}CO\text{–}(NH\text{–}CH_2\text{–}CO)\text{–}NHCH_3} + \underset{\substack{\\ -268.3872059\\ \text{hartree}}}{CH_3\text{–}R} \rightarrow \underset{\text{any conformation}}{CH_3CO\text{–}(NH\text{–}CHR\text{–}CO)\text{–}NHCH_3} + \underset{\substack{\\ -40.5183829\\ \text{hartree}}}{CH_4 + \Delta E^{\text{stabil}}\,(\beta_L)} \quad (2)$$

the propionic acid, χ_1 and χ_2, were rotated with 30.0° increments, producing a total of $12 \times 12 = 144$ points. From the double-scan results, obtained at the RHF/3-21G level of theory, preliminary estimates were made of where possible conformers might be found. Tight geometry optimizations were then performed at the RHF/6-31G(d) and B3LYP/6-31G(d) levels of theory using Berny Optimization: FOPT = TIGHT, Z-Matrix; producing at termination a gradient of less than 1.5×10^{-5} a.u. for all critical points. In this paper, only the B3LYP/6-31G(d) results are reported.

The stabilization or destabilization energy exerted by the side-chain on the backbone was calculated with the aid of CH_3–CH_2–COOH using the following isodesmic reactions with respect to the γ_L and β_L backbones of the glycine residue again quoting only the B3LYP/6-31G(d) energy values:

see equations (1, 2) above

where CH_3–R stands for CH_3–CH_2–COOH and CH_3CO–(NH–CHR–CO)–$NHCH_3$ stands for N-acetyl-*L*-aspartic acid N′-methylamide respectively. An example of the stabilization energy calculation is illustrated in Figure 6. Note that the two stabilization energy values are shifted with respect to each other by 1.13 kcal/mol, which corresponds to the difference of relative energy of the β_L conformation of glycine diamide with respect to its γ_L backbone conformation

$$\Delta E^{\text{stabil}}(\beta_L) - \Delta E^{\text{stabil}}(\gamma_L) = 1.13 \text{ kcal/mol}. \quad (3)$$

In the past, the $\Delta E^{\text{stabil}}(\gamma_L)$ was favoured as most single amino acid diamides have their global minima at γ_L in the gas phase. However, the fully extended β_L conformation is more symmetrical and it is a unique structure on the Ramachandran map. Consequently, ΔE^{stabil} (β_L) is becoming a more accepted parameter [46–48].

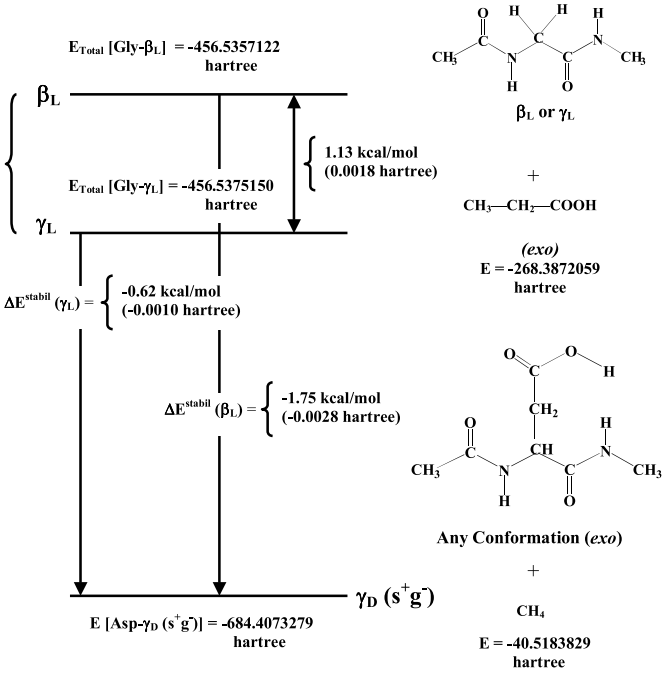

Fig. 6. Definition of stabilization energies of N-acetyl glycine N′ methylamide with respect to the γ_L or β_L conformers of N-acetyl-*L*-aspartic acid N′-methylamide. This is a schematic illustration and the diagram is not to scale.

3 Results and discussion

The side-chain PESs, $E = E(\chi_1, \chi_2)$, were first generated for each one of the nine backbone conformations (γ_L, β_L, δ_L, α_L, γ_D, δ_D, α_D, ε_D) of N-acetyl-*L*-aspartic acid N′-methylamide. These PESs revealed numerous minima, shown in landscape representation (Fig. 7) and contour representation (Fig. 8). However, subsequent optimizations on these apparent minima revealed that only some were true minima. Since the torsional angles ϕ and ψ were frozen, such discrepancy may well be expected. In addition, in a double-scan such as $E = E(\chi_1, \chi_2)$, grid points are optimized at fixed χ_1 and χ_2 values. As a result, these semi-rigid optimizations do not precisely correspond to "true" optimized structures where any minimum appearing on a surface may not be a minimum on the hypersurface. Such "false" minima may represent higher order critical points such as transition structures. Also, a minimum appearing on a surface may be shifted somewhat to a regional neighbour. After the optimization process, all minima were categorized as either "converged" or "not found", shown in Table 1. The position of the minima which were located successfully (*i.e.* "converged") during the optimization process are also shown by arrows in Figures 7 and 8. All optimized dihedral angles, including the relative energies and stabilization energies, are shown in Table 2 where only 27 out of the 81 expected structures were found.

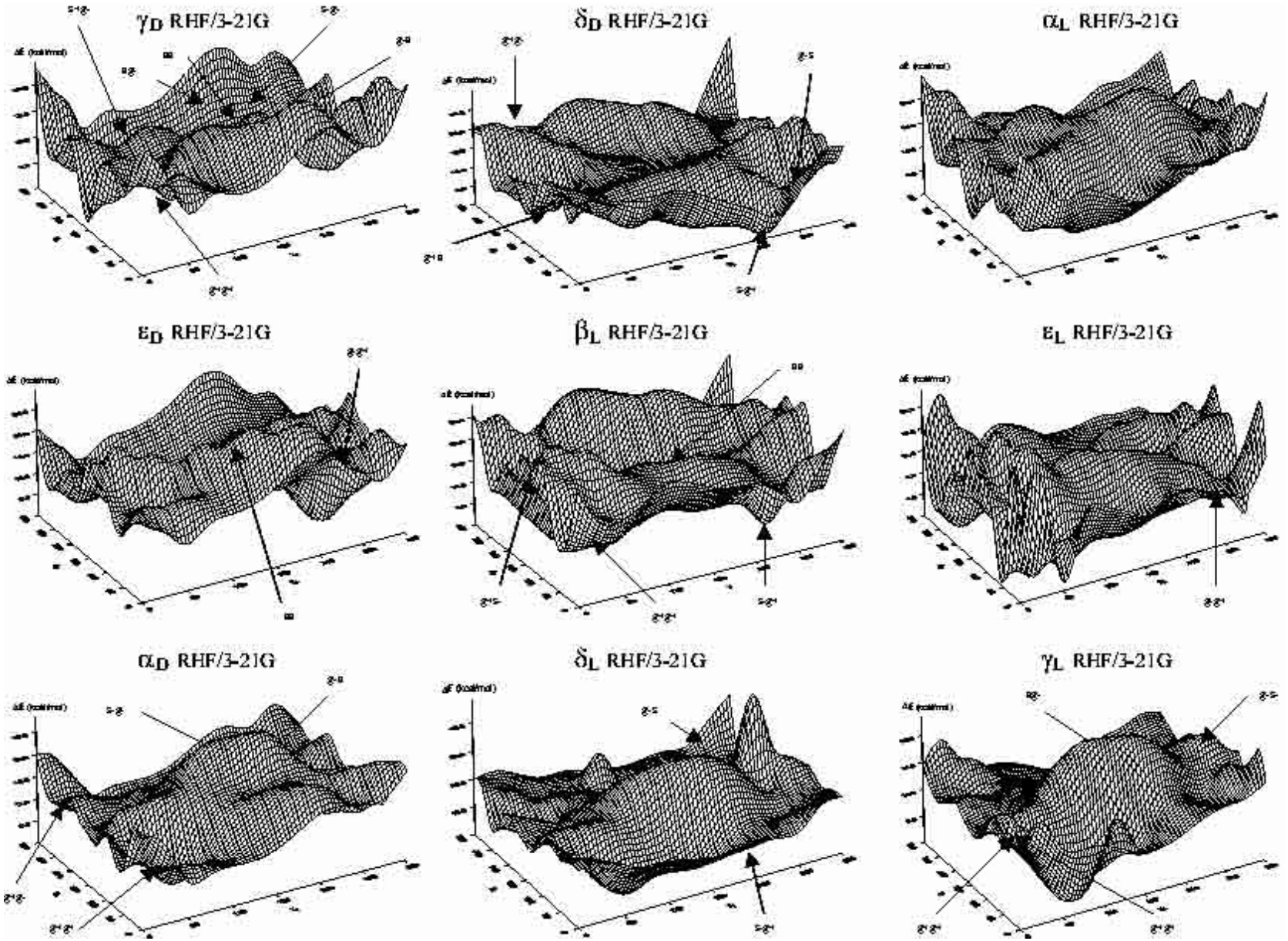

Fig. 7. Landscape representation of the nine side-chain conformational PEHSs, $E = E(\chi_1, \chi_2)$ associated with each one of the nine backbone conformations for N-acetyl-*L*-aspartic acid N′-methylamide. Torsional angles χ_1 and χ_2 are given in degrees.

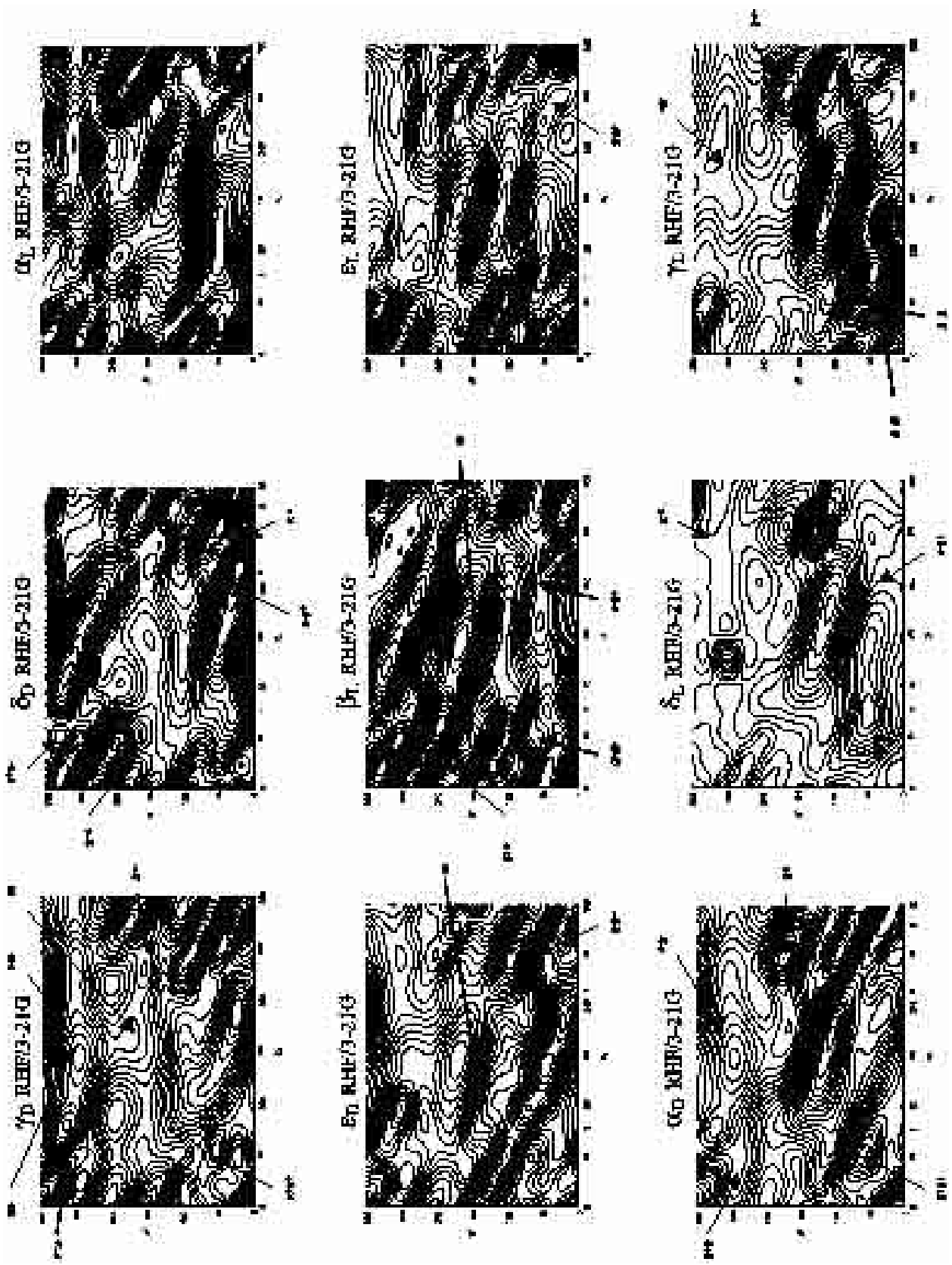

Fig. 8. Contour representation of the nine side-chain conformational PEHSs, $E = E(\chi_1, \chi_2)$ associated with each one of the nine backbone conformations for N-acetyl-*L*-aspartic acid N′-methylamide. Torsional angles χ_1 and χ_2 are given in degrees.

Table 1. A summary of all conformers "converged" or "not found" for N-acetyl-*L*-aspartic acid N′-methylamide in its *exo* form for all its stable backbone (γ_L, β_L, δ_L, α_L, ε_L, γ_D, δ_D, α_D, and ε_D) conformation computed at the B3LYP/6-31G(d) level of theory.

BB	Initial		Final		Convergence	BB	Initial		Final		Convergence	BB	Initial		Final		Convergence
	χ_1	χ_2	χ_1	χ_2			χ_1	χ_2	χ_1	χ_2			χ_1	χ_2	χ_1	χ_2	
γ_L	g^+	g^+	g^+	g^+	Converged	α_L	g^+	g^+	-	-	*Not Found*	δ_D	g^+	g^+	-	-	*Not Found*
γ_L	g^+	*a*	g^+	g^+	Converged	α_L	g^+	*a*	-	-	*Not Found*	δ_D	g^+	*a*	g^+	*a*	Converged
γ_L	g^+	g^-	-	-	*Not Found*	α_L	g^+	g^-	-	-	*Not Found*	δ_D	g^+	g^-	g^+	g^-	Converged
γ_L	*a*	g^+	-	-	*Not Found*	α_L	*a*	g^+	-	-	*Not Found*	δ_D	*a*	g^+	s^-	g^+	Converged
γ_L	*a*	*a*	-	-	*Not Found*	α_L	*a*	*a*	-	-	*Not Found*	δ_D	*a*	*a*	-	-	*Not Found*
γ_L	*a*	g^-	*a*	g^-	Converged	α_L	*a*	g^-	-	-	*Not Found*	δ_D	*a*	g^-	-	-	*Not Found*
γ_L	g^-	g^+	-	-	*Not Found*	α_L	g^-	g^+	-	-	*Not Found*	δ_D	g^-	g^+	g^-	*s*	Converged
γ_L	g^-	*a*	g^-	s^-	Converged	α_L	g^-	*a*	-	-	*Not Found*	δ_D	g^-	*a*	-	-	*Not Found*
γ_L	g^-	g^-	-	-	*Not Found*	α_L	g^-	g^-	-	-	*Not Found*	δ_D	g^-	g^-	-	-	*Not Found*
β_L	g^+	g^+	g^+	g^+	Converged	ε_L	g^+	g^+	-	-	*Not Found*	α_D	g^+	g^+	g^+	g^+	Converged
β_L	g^+	*a*	-	-	*Not Found*	ε_L	g^+	*a*	-	-	*Not Found*	α_D	g^+	*a*	-	-	*Not Found*
β_L	g^+	g^-	g^+	s^-	Converged	ε_L	g^+	g^-	-	-	*Not Found*	α_D	g^+	g^-	g^+	g^-	Converged
β_L	*a*	g^+	s^-	g^+	Converged	ε_L	*a*	g^+	-	-	*Not Found*	α_D	*a*	g^+	-	-	*Not Found*
β_L	*a*	*a*	*a*	*a*	Converged	ε_L	*a*	*a*	-	-	*Not Found*	α_D	*a*	*a*	-	-	*Not Found*
β_L	*a*	g^-	-	-	*Not Found*	ε_L	*a*	g^-	-	-	*Not Found*	α_D	*a*	g^-	s^-	g^-	Converged
β_L	g^-	g^+	-	-	*Not Found*	ε_L	g^-	g^+	g^-	g^+	Converged	α_D	g^-	g^+	-	-	*Not Found*
β_L	g^-	*a*	-	-	*Not Found*	ε_L	g^-	*a*	-	-	*Not Found*	α_D	g^-	*a*	g^-	*a*	Converged
β_L	g^-	g^-	-	-	*Not Found*	ε_L	g^-	g^-	-	-	*Not Found*	α_D	g^-	g^-	-	-	*Not Found*
δ_L	g^+	g^+	-	-	*Not Found*	γ_D	g^+	g^+	g^+	g^+	Converged	ε_D	g^+	g^+	-	-	*Not Found*
δ_L	g^+	*a*	-	-	*Not Found*	γ_D	g^+	*a*	-	-	*Not Found*	ε_D	g^+	*a*	-	-	*Not Found*
δ_L	g^+	g^-	-	-	*Not Found*	γ_D	g^+	g^-	s^+	g^-	Converged	ε_D	g^+	g^-	-	-	*Not Found*
δ_L	*a*	g^+	s^-	g^+	Converged	γ_D	*a*	g^+	-	-	*Not Found*	ε_D	*a*	g^+	-	-	*Not Found*
δ_L	*a*	*a*	-	-	*Not Found*	γ_D	*a*	*a*	*a*	*a*	Converged	ε_D	*a*	*a*	*a*	*a*	Converged
δ_L	*a*	g^-	-	-	*Not Found*	γ_D	*a*	g^-	*a*	g^-	Converged	ε_D	*a*	g^-	-	-	*Not Found*
δ_L	g^-	g^+	-	-	*Not Found*	γ_D	*a*	g^-	s^-	g^-	Converged	ε_D	g^-	g^+	g^-	g^+	Converged
δ_L	g^-	*a*	-	-	*Not Found*	γ_D	g^-	g^+	-	-	*Not Found*	ε_D	g^-	*a*	-	-	*Not Found*
δ_L	g^-	g^-	g^-	*s*	Converged	γ_D	g^-	*a*	g^-	*a*	Converged	ε_D	g^-	g^-	-	-	*Not Found*
						γ_D	g^-	g^-	-	-	*Not Found*						

When examining the optimized values in Table 2, it is shown that when the planar –COOH moiety was rotated against the tetrahedral β-carbon (χ_2), sometime there exist noticeable shifts in the torsional angle away from the typical g^+ value (60°) or from the typical g^- value (−60°) toward the *anti* orientation (+180° or −180° respectively). Such values that fell within the range of +90° and +150° (*i.e.* +120° ± 30°) were labelled as $syn^+(s^+)$, indicating that the oxygen of –OH in the carboxyl moiety was in an *syn* orientation arrangement with the proton attached to the β-carbon, positioned at about +120°. Similarly, values that fell within the range of −90° and −150° (*i.e.* −120° ± 30°) were labelled as $syn^-(s^-)$, indicating that the –OH oxygen of the carboxyl moiety was in *syn* orientation with the proton attached to the β-carbon, positioned at about −120°. It is interesting to note that a g^-g^+ side-chain conformer, shown in Figure 9, was found in the ε_L backbone conformation, a backbone that is not known to harbour stable conformers. In this particular g^-g^+ conformer, it is found that a backbone-backbone internal hydrogen bond, calculated to be 2.297 Å, may be the stabilizing energy needed by the conformer to remain stable. In addition, a rather unusual hydrogen

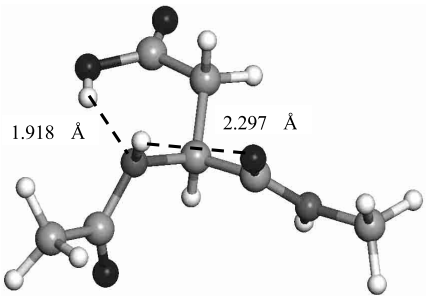

Fig. 9. A pictorial representation of the stable conformer found at g^-g^+ of the ε_L backbone.

bond, $H^{19}\cdots N^2$, which has an intermolecular distance of 1.918 Å (result not tabulated but shown in Fig. 9), may also contribute to the stabilizing force that allows for the existence of this ε_L [g^-g^+] conformer. Figure 10 illustrates the various traditional hydrogen bonds that may exist in the *exo* form of N-acetyl-*L*-aspartic acid N′-methylamide. In this case, since the carboxyl group in the side-chain is in the *exo* form, there is no side-chain-side-chain interaction in the aspartic acid residue. Still, there exist two kinds of stabilizing hydrogen bonds: backbone-backbone (BB/BB) or side-chain-backbone (SC/BB). In total, there are two

Table 2. Optimized conformers of N-acetyl-*L*-aspartic acid N′-methylamide in its *exo* form for all its stable backbone (γ_L, β_L, δ_L, ε_L, γ_D, δ_D, α_D, and ε_D) conformations computed at the B3LYP/6-31G(d) level of theory. Shown here are the optimized torsional angles, computed energy values, relative energies, and stabilization energies.

Final Conform.	Optimized Parameters										
BB [χ_1 χ_2]	ϕ	ψ	ω_0	ω_1	χ_1	χ_2	χ_3	E_{min} (hartree)	ΔE (kcal/mol)	ΔE^{stabil} (kcal) γL	ΔE^{stabil} (kcal) βL
γ_L Backbone Conformation											
γ_L [g^+ g^+]	-81.06	63.58	-171.12	-179.73	50.73	82.28	-13.95	-684.4265160	-0.290	-12.6619	-13.7932
γ_L [g^+ g^+]	-81.91	63.80	-170.70	-179.40	50.58	82.31	-13.98	-684.4266579	-0.379	-12.7509	-13.8822
γ_L [a g^-]	-83.16	64.17	-172.10	-179.20	-165.32	-70.57	4.41	-684.4208809	3.246	-9.1258	-10.2571
γ_L [g^- s^-]	-84.07	70.53	-169.26	-176.36	-45.91	-121.27	0.59	-684.4126227	8.428	-3.9437	-5.0750
β_L Backbone Conformation											
β_L [g^+ g^+] [a,b]	-156.59	-176.43	177.82	-171.12	64.56	72.14	-1.65	-684.4058456	12.681	0.3090	-0.8223
β_L [g^+ s^-]	158.11	-139.74	172.36	179.88	63.71	-90.93	6.92	-684.4201077	3.731	-8.6406	-9.7719
β_L [s^- g^+]	-169.92	-177.45	175.01	-179.22	-130.05	74.37	-4.45	-684.4237651	1.436	-10.9357	-12.0669
β_L [a a]	-167.29	170.92	174.39	179.24	-159.70	167.29	-3.78	-684.4161709	6.202	-6.1702	-7.3015
δ_L Backbone Conformation											
δ_L [s^- g^+] [a,b]	-161.43	45.11	-176.35	173.71	-118.31	48.09	4.66	-684.4099383	10.113	-2.2592	-3.3905
δ_L [g^- s]	-135.40	25.16	-177.58	174.07	-67.01	-15.76	14.84	-684.4103060	9.882	-2.4900	-3.6212
ε_L Backbone Conformation											
ε_L [g^- g^+]	-94.47	149.36	160.78	177.79	-63.25	43.99	-5.09	-684.4102974	9.888	-2.4846	-3.6158
γ_D Backbone Conformation											
γ_D [g^+ g^+]	64.96	-61.81	168.52	175.34	60.23	67.68	-17.12	-684.4033200	14.266	1.8938	0.7625
γ_D [s^+ g^-]	79.72	-53.75	-177.65	-174.22	107.66	-75.40	6.66	-684.4073279	11.751	-0.6212	-1.7524
γ_D [a a]	74.38	-70.80	-179.62	175.29	-154.73	-154.72	4.80	-684.4035338	14.132	1.7597	0.6284
γ_D [a g^-]	70.34	-81.17	177.02	172.78	-176.52	-70.85	4.12	-684.4078146	11.446	-0.9266	-2.0579
γ_D [s^- g^-]	70.12	-28.28	167.77	-175.15	-143.16	-35.94	-3.53	-684.4144381	7.289	-5.0829	-6.2142
γ_D [g^- a]	73.63	-44.57	167.30	-177.58	-63.68	176.48	-0.54	-684.4098022	10.198	-2.1738	-3.3051
δ_D Backbone Conformation											
δ_D [g^+ a] [a,b]	-160.74	-48.85	175.72	-176.93	52.48	-164.30	3.41	-684.4071457	11.865	-0.5068	-1.6381
δ_D [g^+ g^-] [a,b]	-152.24	-46.34	162.79	-174.56	62.86	-42.90	-3.04	-684.4046175	13.452	1.0796	-0.0516
δ_D [s^- g^+]	-166.96	-52.06	172.53	-173.85	-121.06	55.27	4.53	-684.4070418	11.930	-0.4416	-1.5729
δ_D [g^- s] [a,b]	-135.56	-70.97	168.84	-177.26	-79.12	2.05	12.10	-684.4055002	12.898	0.5257	-0.6055
α_D Backbone Conformation											
α_D [g^+ g^+]	51.02	50.87	158.65	-173.41	57.95	78.07	-13.34	-684.4118612	8.906	-3.4659	-4.5971
α_D [g^+ g^-]	49.91	35.67	175.22	-176.17	42.68	-69.95	7.37	-684.3904410	22.348	9.9755	8.8442
α_D [s^- g^-]	68.57	27.90	165.45	-178.48	-147.48	-61.61	0.62	-684.4145135	7.242	-5.1302	-6.2615
α_D [g^- a]	66.58	30.54	164.64	-177.60	-64.08	-177.94	0.92	-684.4094323	10.430	-1.9417	-3.0730
ε_D Backbone Conformation											
ε_D [a a]	68.83	176.68	-157.00	-176.55	-152.00	171.32	-0.35	-684.4069842	11.967	-0.4055	-1.5368
ε_D [g^- g^+]	85.36	163.60	-152.58	178.97	-62.34	93.43	-7.44	-684.4096079	10.320	-2.0519	-3.1832

[a] After 200 iterations under B3LYP/6-31G(d) at (TIGHT, Z-MATRIX), the force has converged, but the displacement did not converge completely.

[b] This result was obtained from an optimization fully converged under regular B3LYP/6-31G(d) at (Z-MATRIX).

Table 3. The relative distances of potential hydrogen bonds of N-acetyl-*L*-aspartic acid N′-methylamide in its *exo* form for all its stable backbone (γ_L, β_L, δ_L, ε_L, γ_D, δ_D, α_D, and ε_D) conformations computed at the B3LYP/6-31G(d) level of theory. No conformers were found for the α_L backbone and hence no hydrogen bond distances for the α_L backbone could be tabulated.

Final Conform.	Interaction Type		Distance (Å)							
BB [$\chi_1\chi_2$]	BB/BB	SC/BB	H9-O5	H9-O17	H9-O18	H19-O5	H6-O10	H6-O17	H6-018	H19-O10
γ_L Backbone Conformation										
γ_L [g^+g^+]	1B	2C	3.906	2.344	3.376	1.749	1.917	5.528	5.068	5.421
γ_L [g^+g^+]	1B	2C	3.899	2.342	3.371	1.748	1.916	5.515	5.065	5.430
γ_L [$a\ g^-$]	1B	2C	3.776	4.780	4.809	1.746	1.940	5.610	4.866	5.454
γ_L [g^-s^-]	1B	2A	3.880	2.044	3.796	4.863	1.929	5.381	5.973	5.902
β_L Backbone Conformation										
β_L [g^+g^+] [a,b]	1A	-	2.175	3.850	3.943	3.124	5.015	4.888	3.465	5.396
β_L [g^+s^-]	1A	2D, 2F	2.156	4.717	4.271	5.117	5.000	1.977	3.699	1.717
β_L [s^-g^+]	1A	2F	2.133	5.371	4.819	5.168	5.023	2.434	3.829	1.827
β_L [$a\ \ a$]	1A	2D	2.046	4.983	5.598	5.767	5.090	1.937	3.847	4.422
δ_L Backbone Conformation										
δ_L [s^-g^+] [a,b]	-	2F	3.532	5.467	4.663	4.779	4.121	5.934	5.150	1.773
δ_L [$g^-\ s$]	-	2F	3.844	4.562	4.047	4.677	3.770	6.205	5.302	1.841
ε_L Backbone Conformation										
ε_L [g^-g^+]	1A	-	2.297	4.853	3.402	4.295	4.115	5.002	5.195	3.253
γ_D Backbone Conformation										
γ_D [g^+g^+]	1B	-	4.044	4.364	4.806	3.506	1.810	4.106	2.731	3.086
γ_D [s^+g^-]	1B	2F	3.776	5.537	4.829	4.588	2.225	3.746	2.565	1.713
γ_D [$a\ \ a$]	1B	-	3.677	4.549	5.637	5.103	1.975	4.773	4.615	4.654
γ_D [$a\ g^-$]	1B	-	3.678	5.186	5.266	3.181	1.934	4.846	3.378	3.970
γ_D [s^-g^-]	1B	2C	4.214	4.995	4.763	1.716	1.896	5.732	4.943	5.059
γ_D [$g^-\ a$]	1B	-	4.140	2.740	4.465	5.415	1.876	5.060	5.391	4.661
δ_D Backbone Conformation										
δ_D [$g^+\ a$] [a,b]	-	2D	3.620	3.076	4.641	5.666	4.848	1.942	3.960	4.337
δ_D [g^+g^-] [a,b]	-	2E	3.497	4.848	3.182	4.451	4.853	3.305	2.248	3.376
δ_D [s^-g^+]	-	2F	3.450	5.599	4.753	4.740	4.693	5.019	5.204	1.745
δ_D [$g^-\ s$] [a,b]	-	2F	3.425	5.149	4.371	4.654	5.131	4.703	5.027	1.717
α_D Backbone Conformation										
α_D [g^+g^+]	-	2C	4.422	3.685	4.547	1.812	3.005	5.525	4.956	3.173
α_D [g^+g^-]	-	-	4.430	4.908	3.525	4.794	2.764	5.396	5.086	3.222
α_D [s^-g^-]	-	2C	4.438	4.677	4.988	1.711	3.000	6.042	5.158	4.608
α_D [$g^-\ a$]	-	-	4.435	2.514	4.288	4.733	3.024	5.034	6.237	4.866
ε_D Backbone Conformation										
ε_D [$a\ \ a$]	-	2D	2.792	4.800	5.647	5.834	4.824	1.986	3.740	4.491
ε_D [g^-g^+]	-	2F	2.727	4.660	4.241	4.776	5.273	4.242	5.246	1.760

[a] After 200 iterations under B3LYP/6-31G(d) at (TIGHT, Z-MATRIX), the force has converged, but the displacement did not converge completely.

[b] This result was obtained from an optimization fully converged under regular B3LYP/6-31G(d) at (Z-MATRIX).

BB/BB hydrogen bond interactions and six SC/BB hydrogen bond interactions. The corresponding distances for these hydrogen bond interactions are tabulated in Table 3. It is also interesting to note that almost all stable conformers, with the exception of g^+g^- and g^-a in the α_D conformation, there exist at least one type of hydrogen bond interaction. This may suggest that hydrogen bonding, at least in part, contribute significantly to the stability of a conformer for the aspartic acid residue. Here, the BB/BB interaction can be considered as an internal stabilizing factor that allows fundamental stability for the aspartic acid residue while at the same time allowing the side-chain to participate in external interactions with other substrates. On the other hand, the SC/BB interaction can induce even greater internal stability to the aspartic acid residue. An example to illustrate this phenomenon exists in the γ_L [ag^-] conformation where type 1B (BB/BB) and type 2C (SC/BB) of the hydrogen bond interactions seems to contribute major stabilizing forces that allow for the existence of the conformer at this particular backbone.

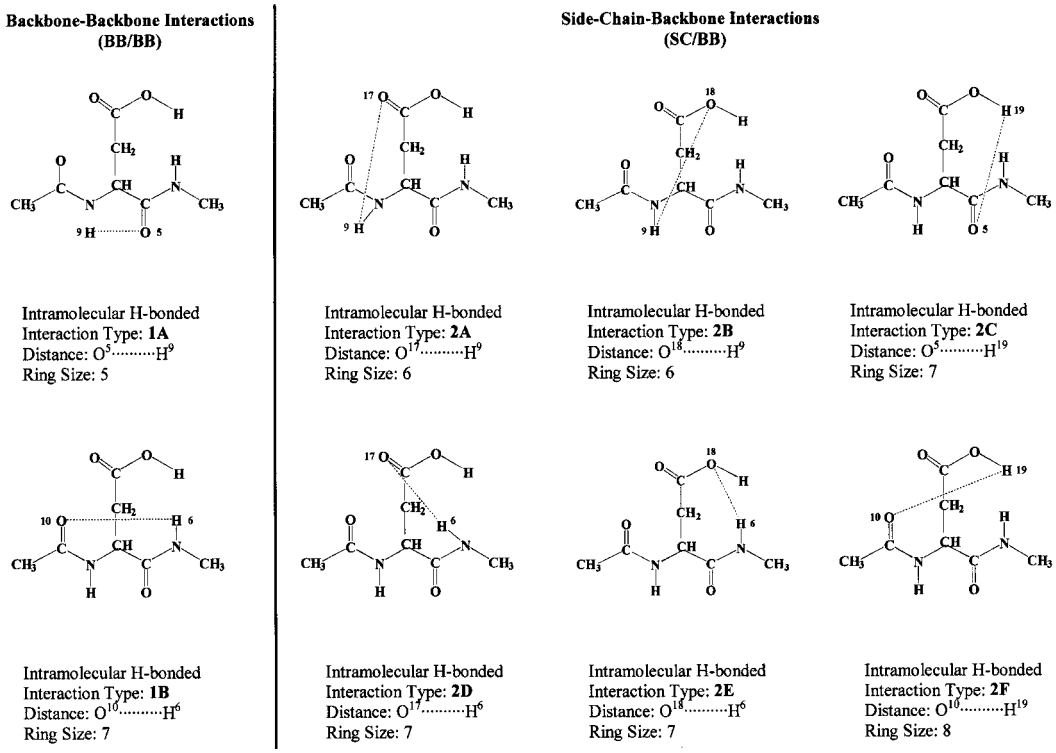

Fig. 10. Classification of the types of internal hydrogen bonding for N-acetyl-*L*-aspartic acid N′-methylamide.

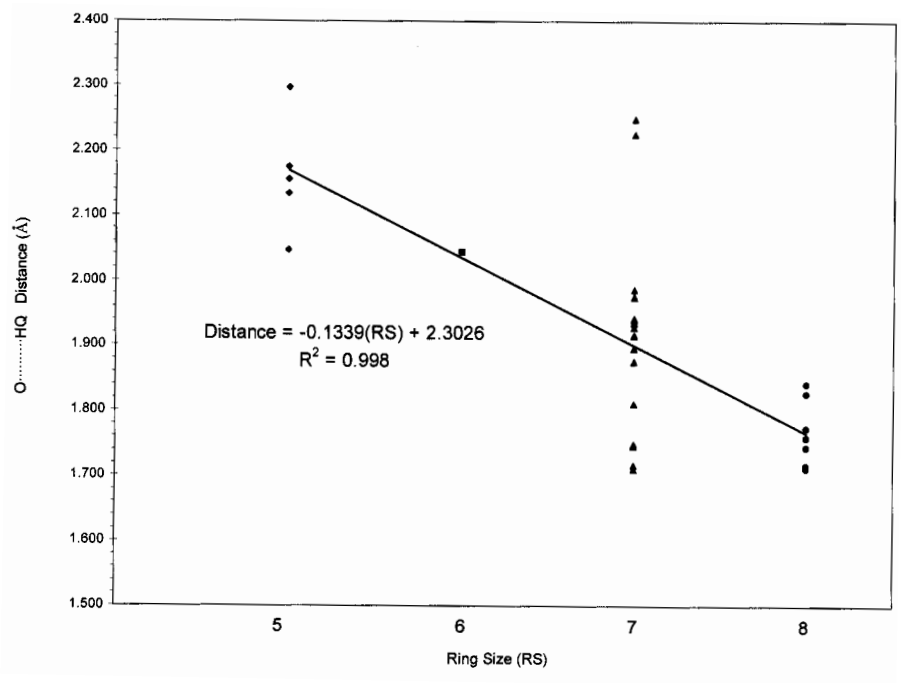

Fig. 11. A trend showing the interrelation between hydrogen-bonded distance and ring size (RS) of internal hydrogen bonds of N-acetyl-*L*-aspartic acid N′-methylamide. Note: HQ may be H–N or H–O.

A correlating trend between hydrogen bond distance and ring size (RS) is shown in Figure 11. Here, it is apparent that the shorter the hydrogen bond distance, the greater the RS. The overall correlation equation shows a least square value of $R^2 = 0.998$, showing convincingly that such trend is significant. We did not observe any Type 2B hydrogen interactions for the aspartic acid residue.

In Figure 12, various stabilization energies, with respect to either β_L or γ_L of the glycine residue, are shown in a bar-graph format. The difference in stabilization energy, ΔE^{stabil}, with respect to β_L and with respect to γ_L is constant (1.13 kcal/mol), as shown in Figure 5. Consequently, it is enough to discuss only one set of the stabilization energy data. Here, we choose to discuss the values

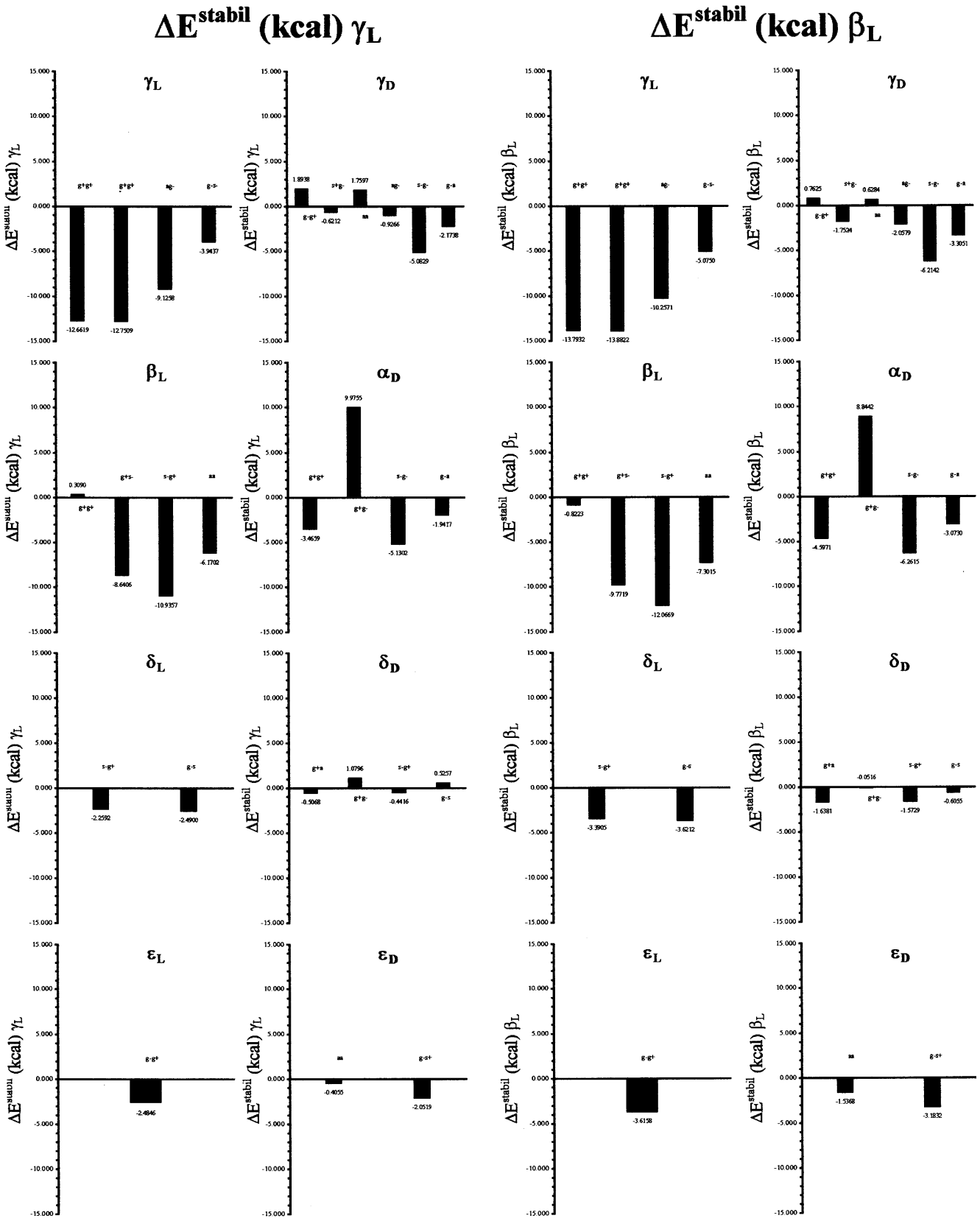

Fig. 12. Computed stabilization energies of N-acetyl-*L*-aspartic acid N′-methylamide with respect to γ_L and β_L backbone conformation of N-acetyl-*L*-aspartic acid N′-methylamide.

with respect to the γ_L glycine residue. One can observe that the L subscripted conformations (*i.e.* β_L, δ_L, ε_L, γ_L) of the aspartic acid residue are stabilized more extensively than its D subscripted forms (*i.e.* α_D, γ_D, δ_D, ε_D). As illustrated in Figure 12, most of the stabilization energies for the L conformers, having a more negative value, indicated that the conformers are truly stabilized. This is shown by the fact that stable L subscripted conformers for N-acetyl-*L*-aspartic acid N′-methylamide either have great negative values or small positive values for their stabilization energies. This trend is observed in the γ_L, β_L, δ_L and ε_L backbones for the aspartic acid residue. On the other hand, most conformers found for the D subscripted form of the aspartic acid residue are de-stabilized. Again, the D-subscripted conformers, shown in Figure 12, have either great positive values or small negative values for their stabilization energies. This trend exists in the α_D, γ_D, δ_D and ε_D backbones for the aspartic acid residue. Even though the ε_L and the ε_D conformers seem to represent an apparent exception to the trend (where both L and D subscripted conformers appeared to be stabilized), nevertheless, the actual magnitudes for their ΔE^{stabil} still followed the trend outlined above.

We also observed that in some cases, the ω_0 torsional angle of the stable conformers (such as those found in the α_D conformation) deviated from the ideal value of 180°. One possible reason for such apparent discrepancy is that there exist strong hydrogen bond interactions that act as stabilizing forces in these conformers. For example, in the α_D [g^+g^+] conformation as well as in *aa* and g^-g^+ of the ε_D conformation, where the ω_0 torsional angle deviates the most from the ideal, there exist strong SC/BB interactions (*i.e.* having hydrogen bond lengths of less than 2.000 Å). This may suggest that as the conformer seeks a stabilizing force, it is willing to rotate its terminal methyl groups, changing its ω_0 torsional angles, in order to form a hydrogen bond interaction that is strong enough to stabilize itself. Also, such observation from the optimization results for N-acetyl-*L*-aspartic acid N′-methylamide may provide insights on the aspartyl residue's role in the intramolecular interactions of RGD. Such an example may be found in the conformers of the δ_L, δ_D, α_D and ε_D conformations, which possess the SC/BB interactions shown in Table 3. Meanwhile, it is reasonable to infer that an ideal stabilizing situation for the aspartyl residue in a peptide chain would involve both BB/BB as well as SC/BB being present. In γ_L, β_L, and γ_D conformations, such instances of having both BB/BB and SC/BB interactions exist. Interestingly, these three backbones are traditionally recognized as where most of the stable conformers for an amino acid would be found in the gas phase. The study of SC/BB and BB/BB interactions in N-acetyl-*L*-aspartic acid N′-methylamide may deem significant as these interactions may represent the internal stabilizing force within a peptide chain when it is binded to a substrate, such as a receptor (charged or uncharged). The fact that 19 out of the 27 optimized conformers for the *exo* form of N-acetyl-*L*-aspartic acid N′-methylamide possess a SC/BB interaction suggest that the ability of the aspartic acid residue to form an external hydrogen bond, whether to itself, to an adjacent neighbour or to a binding substrate, may deem significant to the molecule's stability as well as the relative stability of a binding assay involving the amino acid.

4 Conclusions

Using quantum chemical calculations at the B3LYP/6-31G(d) *ab initio* level, the conformational preferences for the *exo* form of N-acetyl-*L*-aspartic acid-N′-methylamide were determined. We found and optimized a total of 27 stable conformers (out of the possible 81) for the aspartic acid residue at this level of theory. All relative energies, including the stabilization exerted by the side-chain on the backbone, were calculated for the 27 stable conformers.

Various BB/BB (N–H···O=C) and BB/SC (N–H···O=C; N–H···OH) hydrogen bonds were analyzed. There was no SC/SC interaction in the carboxyl group of the aspartic acid residue, indicating that the side-chain may be involved with external hydrogen bonding to stabilize the amino acid. A total of two BB/BB interactions and six SC/BB interactions were identified amongst the stable conformers. However, only five of the possible six SC/BB interactions were observed. In addition, 25 of the 27 conformers exhibited at least one or more hydrogen bond types. External hydrogen interactions are significant when the aspartyl residue participates in intra- or inter-molecular interactions in polypeptides, such as in the RGD tripeptide. In the case of RGD, the presence or absence of these external stabilizing forces will directly affect the folding or unfolding of the tripeptide moiety.

In this work, the stable g^-g^+ conformer found at the ε_L backbone may represent a novel geometry in which the aspartyl residue may arrange itself during such peptide folding.

The authors would like to express their gratitude for the generous allocation of CPU time provide by the National Cancer Institute (NCI) at the Frederick Biomedical Supercomputing Center.

References

1. E. Ruoslahti, M.D. Pierschbacher, Science **238**, 491 (1987)
2. A. Horster, B. Teichmann, R. Hormes, D. Grimm, J. Kleinschmidt, G. Sczakiel, Gen. Ther. **6**, 1231 (1998)
3. R.T. Inouye, E.F. Terwilliger, J. Virol. **71**, 4071 (1997)
4. M.K. Magnusson, S.S. Hong, P. Boulanger, L. Lindholm, J. Virol. **75**, 7280 (2001)
5. N. Okada *et al.*, Biochem. Biophys. Res. Commun. **282**, 173 (2001)
6. C. Hay *et al.*, J. Vasc. Res. **38**, 315 (2001)
7. C.D. Anuradha, S. Kanno, S. Hirano, Cell Biol. Toxicol. **16**, 275 (2000)
8. K. Kuroda *et al.*, Cancer Lett. **159**, 33 (2000)
9. H. Ghandehari, R. Sharan, W. Rubas, W.M. Killing, J. Pharm. Pharm. Sci. **4**, 32 (2001)

10. S. Hatse *et al.*, Mol. Pharmacol. **60**, 164 (2001)
11. J. Rotonda *et al.*, Chem. Biol. **8**, 357 (2001)
12. C. Demougeot *et al.*, J. Neurochem. **77**, 408 (2001)
13. M.J. Collins, E.R. Waite, A.C. van Duin, Philos. Trans. R. Soc. Lond. B. Biol. Sci. **354**, 51 (1999)
14. C.M. Deane, F.H. Allen, R. Taylor, T.L. Blundell, Protein Eng. **12**, 1025 (1999)
15. A. Heine *et al.*, Science **279**, 1934 (1998)
16. J.A. Contreras, M. Karlsson, T. Østerlund, H. Laurell, A. Svensson, C. Holm, J. Biol. Chem. **271**, 31426 (1996)
17. R. Hoffmann, D.J. Craik, K. Bokonyi, I. Varga, L. Otvos Jr, J. Pept. Sci. **5**, 442 (1999)
18. D. Saadat, D.H. Harrison, Biochemistry **37**, 10074 (1998)
19. R. Hu, J. Bekisz, H. Schmeisser, P. McPhie, K. Zoon, J. Immunol. **167**, 1482 (2001)
20. G.F. Short 3rd, A.L. Laikhter, M. Lodder, Y. Shayo, T. Arslan, S.M. Hecht, Biochemistry **39**, 8768 (2000)
21. H.G. Wiker, M.A. Wilson, G.K. Schoolnik, Microbiology **146**, 1525 (2000)
22. L.S. Brown, R. Needleman, J.K. Lanyi, Biochemistry **38**, 6855 (1999)
23. S.J. Salpietro, A. Perczel, Ö. Farkas, R.D. Enriz, I.G. Csizmadia, J. Mol. Struct. (Theochem) **497**, 39 (2000)
24. A. Perczel *et al.*, J. Am. Chem. Soc. **113**, 6256 (1991)
25. M.A. McAllister, A. Perczel, P. Császár, W. Viviani, J.L. Rivail, I.G. Csizmadia, J. Mol. Struct. (Theochem) **288**, 161 (1993)
26. M.A. McAllister, A. Perczel, P. Császár, I.G. Csizmadia, J. Mol. Struct. (Theochem) **288**, 181 (1993)
27. A. Perczel, M.A. McAllister, P. Császár, I.G. Csizmadia, Can. J. Chem. **72**, 2050 (1994)
28. M. Cheung *et al.*, J. Mol. Struct. (Theochem) **309**, 151 (1994)
29. A.M. Rodriguez *et al.*, J. Mol. Struct. (Theochem) **455**, 275 (1998)
30. A. Perczel, Ö. Farkas, I.G. Csizmadia, J. Am. Chem. Soc. **117**, 1653 (1995)
31. H.A. Baldoni *et al.*, J. Mol. Struct. **500**, 97 (2000) (Millennium Volume)
32. W. Viviani, J.-L. Rivail, A. Perczel, I.G. Csizmadia, J. Am. Chem. Soc. **115**, 8321 (1993)
33. Ö. Farkas, M.A. McAllister, J.H. Ma, A. Perczel, M. Hollósi, I.G. Csizmadia, J. Mol. Struct. (Theochem) **369**, 105 (1996)
34. A. Perczel, Ö. Farkas, I.G. Csizmadia, Can. J. Chem. **75**, 1120 (1997)
35. I. Jakli, A. Perczel, Ö. Farkas, M. Hollosi, I.G. Csizmadia, J. Mol. Struct. (Theochem) **455**, 303 (1998)
36. A. Perczel, Ö. Farkas, I.G. Csizmadia, J. Comp. Chem. **17**, 821 (1996)
37. A. Perczel, Ö. Farkas, I.G. Csizmadia, J. Am. Chem. Soc. **118**, 7809 (1996)
38. I. Jakli, A. Perczel, Ö. Farkas, C.P. Sosa, I.G. Csizmadia, J. Comp. Chem. **21**, 626 (2000)
39. M. Berg, S.J. Salpietro, A. Perczel, Ö. Farkas, I.G. Csizmadia, J. Mol. Struct. (Theochem) **504**, 127 (2000)
40. H.A. Baldoni *et al.*, J. Mol. Struct. (Theochem) **465**, 79 (1999)
41. M.A. Zamora *et al.*, J. Mol. Struct. (Theochem) **540**, 271 (2001)
42. J.C. Vank, C.P. Sosa, A. Perczel, I.G. Csizmadia, Can. J. Chem. **78**, 395 (2000)
43. A. Perczel, I.G. Csizmadia, Int. Rev. Phys. Chem. **14**, 127 (1995)
44. *GAUSSIAN 94, Revision D.2*, M.J. Frisch, G.W. Trucks, H.B. Schlegel, P.M.W. Gill, B.G. Johnson, M.A. Robb, J.R. Cheeseman, T. Keith, G.A. Petersson, J.A. Montgomery, K. Raghavachari, M.A. Al-Laham, V.G. Zakrzewski, J.V. Ortiz, J.B. Foresman, J. Cioslowski, B.B. Stefanov, A. Nanayakkara, M. Challacombe, C.Y. Peng, P.Y. Ayala, W. Chen, M.W. Wong, J.L. Andres, E.S. Replogle, R. Gomperts, R.L. Martin, D.J. Fox, J.S. Binkley, D.J. Defrees, J. Baker, J.P. Stewart, M. Head-Gordon, C. Gonzalez, J.A. Pople, Gaussian, Inc., Pittsburgh Pa, 1995
45. *GAUSSIAN 98, Revision A.x*, M.J. Frisch, G.W. Trucks, H.B. Schlegel, G.E. Scuseria, M.A. Robb, J.R. Cheeseman, V.G. Zakrzewski, J.A. Montgomery, Jr., R.E. Stratmann, J.C. Burant, S. Dapprich, J.M. Millam, A.D. Daniels, K.N. Kudin, M.C. Strain, Ö. Farkas, J. Tomasi, V. Barone, M. Cossi, R. Cammi, B. Mennucci, C. Pomelli, C. Adamo, S. Clifford, J. Ochterski, G.A. Petersson, P.Y. Ayala, Q. Cui, K. Morokuma, D.K. Malick, A.D. Rabuck, K. Raghavachari, J.B. Foresman, J. Cioslowski, J.V. Ortiz, A.G. Baboul, B.B. Stefanov, G. Liu, A. Liashenko, P. Piskorz, I. Komaromi, R. Gomperts, R.L. Martin, D.J. Fox, T. Keith, M.A. Al-Laham, C.Y. Peng, A. Nanayakkara, C. Gonzalez, M. Challacombe, P.M.W. Gill, B.G. Johnson, W. Chen, M.W. Wong, J.L. Andres, M. Head-Gordon, E.S. Replogle, J.A. Pople, Gaussian, Inc., Pittsburgh PA, 1998
46. M. Tarditi *et al.*, J. Mol. Struct. (Theochem) **545**, 29 (2001)
47. M.N. Barroso *et al.*, J. Mol. Struct. (Theochem) **548**, 21 (2001)
48. M.F. Masman *et al.*, J. Mol. Struct. (Theochem) **543**, 203 (2001)
49. M.A. Berg *et al.*, J. Mol. Struct. **500**, 5 (2000) (Millennium Volume)